Proceedings of the Twenty-fifth (2015) International Ocean and Polar Engineering Conference **www.isope.org**
Kona, Big Island, Hawaii, USA, June 21-26, 2015

ISBN 978-1-880653-89-0; ISSN 1098-6189

Experimental study on the ultimate axial anti-slide capacity for a partially-embedded pipeline on the sloping sandy seabed

Ning Wang, Fu-Ping Gao, Cun Hu
Key Laboratory for Mechanics in Fluid Solid Coupling Systems, Institute of Mechanics, Chinese Academy of Sciences, Beijing, China

ABSTRACT

The ultimate anti-slide capacity for a submarine pipeline on the sloping seabed is one of the main concerns in the global buckling design. A mechanical-actuator facility has been designed and constructed for physical modeling of the axial pipe-soil interaction. The phenomenon of "pipe-trembling" was observed in the process of the pipe's axial movement, which is more prone to occur for the smoother pipes. Based on dimensional analyses, a dimensionless factor is proposed to describe the anti-slide capacity of the pipeline on a sloping sandy seabed. Experimental results indicate that both the slope angle and the pipe roughness have much effect on the axial pipe-soil interaction behavior and eventually on the anti-slide capacity. Unlike the lateral pipe-soil interaction, the slope angle has slight effect on the axial soil resistance to the partially-embedded pipeline in the examined range of slope angle ($-9^{o} \sim +9^{o}$).

KEY WORDS: axial pipe-soil interaction; sloping seabed; anti-slide capacity; mechanical actuator modelling.

INTRODUCTION

The axial stress in a submarine pipeline is usually caused by the hydrodynamic loading, thermal loading (Hobbs, 1984), axial component of self-weight and interaction with the neighboring soil etc. During its service life, if the anti-slide capacity of a pipeline cannot balance the axial loads, the axial stress will be accumulated along the pipeline and may finally lead to a pipeline's global buckling (Cheuk et al, 2007). It is crucial to well consider the axial anti-slide capacity for the stability design of a pipeline.

The early investigations on the pipe's axial anti-slide capacity are mostly about buried pipeline, in which the Coulomb friction theory is commonly used. In the study of Schaminee et al. (1990), the pipe-weight, burial depth and the buoyant unit weight of soil are mainly concerned for the axial anti-slide capacity:

$$F_{\mathrm{A}} = 0.25\pi D\mu\left[2\gamma' H + 2K_{\mathrm{a}}\gamma'(H + D/2) + W_{\mathrm{S}}/D\right] \quad (1)$$

in which, K_{a}, γ' are the active lateral pressure coefficient and buoyant unit weight of the soil; D, W_{S}, H are the diameter, submerged weight and buried depth of the pipe respectively; μ is the friction coefficient between the pipe and soil.

Nasser et al. (2011) studied the axial soil resistance coupled with lateral resistance for buried pipelines experimentally and numerically, in which significant coupling effects between the axial and lateral resistance were observed.

Unlike the buried pipeline, many pipelines operating in deep water are partially embedded and lack of fixing measures. The global buckling under axial loads is more likely to occour and it's harder to estimate the mechanism of pipe-soil interaction for a partially embedded pipeline. In recent years, the axial pipe-soil interaction of partially embedded pipelines has received much attention. White & Randolph (2007) proposed a theoretical solution for the axial resistance of the soil under drained conditions:

$$F_{\mathrm{Ru}} = \mu W_{\mathrm{S}} \frac{2\sin\theta}{\theta + \sin\theta\cos\theta} = \mu W_{\mathrm{S}}\kappa \quad (2)$$

Eq. (2) shows that the pipe's settlement angle θ strongly affect the axial resistance (the "wedge effect"). According to the factor of wedge effect κ, the axial resistance of a half-buried pipeline can be 27% larger than that of a non-embedded pipeline.

The "rate effect" has become another focus for the axial resistance of partially embedded pipeline on cohesive soil. The study by Randolph et al. (2012) indicated that the axial resistance was strain-rate dependent under different drainage conditions. For undrained condition, the axial soil-resistance decreased due to the excess pore pressure generated in the adjacent soil (i.e., the shear band). A dimensionless coefficient VD/C_{V}, in which V is the axial velocity of the pipe and C_{V} is the soil's consolidation coefficient, was used to distinguish the drainage condition. Chatterjee et al (2013) assumed that when $VD/C_{\mathrm{V}} < 0.1$, the pipe-soil interaction was in drained condition, when $VD/C_{\mathrm{V}} > 100$,it was under undrained condition. Quinn & Brown (2011) clarified that for higher strain-rate cases, the axial resistance may increase with strain-rate under undrained condition because of the viscous effect of soil.

For the pipeline laid on a sloping seabed (e.g. the continental slope),

recent studies have shown that the slope angle makes it more complicate for estimating the stability along the slope. Gao et al. (2012) experimentally studied the lateral stability of the pipeline on a sloping sandy seabed. The results indicated that the slope not only affected the component of pipe-weight along the slope, but greatly influenced the mechanism of pipe-soil interaction and the coefficient of soil resistance η. However, the factor of slope angle has not been considered in existing recommended practices (Det Norske 2010). Besides, the effect of slope angle on the axial anti-slide capacity is far from well-understood.

The present experimental study focuses on the axial pipe-soil interaction and corresponding anti-slide capacity for the partially embedded pipeline along a sloping sandy seabed. A mechanical actuator facility was designed and constructed for physical modeling of axial pipe-soil interactions. The effects of slope angle, pipe roughness and submerged pipe-weight are investigated experimentally.

DIMENSIONAL ANALYSIS

For a submarine pipeline laid along a sloping seabed, the axial pipe-soil interaction involves the external axial loading (F_{Du}) mainly due to the thermal or hydrodynamic effects, the ultimate soil resistance (F_{Ru}) provided by the neighboring soil, the axial component of submerged pipe weight ($W_S \sin\alpha$), etc (see Fig.1).

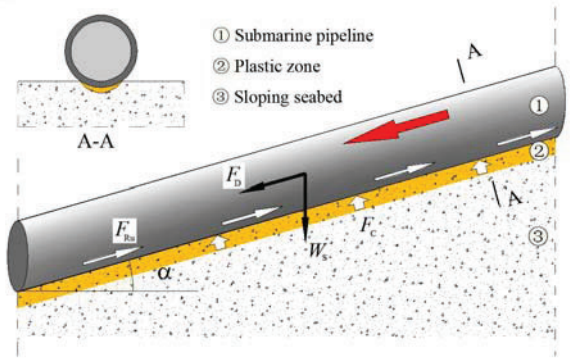

Fig.1 Illustration of the axial pipe-soil interaction along a sloping seabed.

The soil resistance F_{Ru} is affected by the normal contact force between the pipe and the soil, the pipe roughness and the size of sand grains. It also depends on the settlement of the pipe, the shearing velocity, the consolidation coefficient and internal friction angle of the soil. The anti-slide capacity can be expressed as follows:

$$F_A = F_{Ru} + W_S \sin\alpha = f(W_S, d_s, D, d_p, V, \alpha, \gamma', C_V, \phi, w_0, ...) \quad (3a)$$

in which, d_p represents the pipe roughness (in this study, d_p is the mean particle size of pipe surface); d_s is the diameter of sand grains (in this study, $d_s = d_{50}$); α is the slope angle; ϕ is the internal friction angle of soil; w_0 is the initial average embedment of the pipe, which is the vertical distance between the original mudline to the bottom of the pipe.

Eq.(3a) can be further expressed in the following dimensionless form:

$$\zeta = f'(G, \frac{VD}{C_V}, \frac{D}{d_s}, \lambda, \alpha, \phi, \frac{w_0}{D}, ...) \quad (3b)$$

where, ζ is the axial anti-slide capacity factor, which is defined as the ratio of axial anti-slide capacity F_A to the normal contact force F_C ($F_C = W_S \cos\alpha$), i.e., $\zeta = F_{Ru} / (W_S \cos\alpha) + \tan\alpha$; G is the dimensionless submerged pipe-weight, which is expressed as $G = W_S / (D^2 \gamma')$; λ is the relative roughness of pipe-soil interface, which is expressed as $\lambda = d_p / d_{50}$, d_{50} is the mean size of sand grains.

In this study, the effects of relative roughness λ, slope angle α and submerged weight of the pipe (G) on the anti-slide capacity factor ζ is examined experimentally.

EXPERIMENTAL SETUPS

As illustrated in Fig.2, the mechanical-actuator system was located on a sand box, which was specially designed for structure-soil interaction tests. The dimension of the stainless steel sand box was 5.0 m long, 1.0 m wide, 1.5 m high. And the side wall of the test section was made of toughened glass, which made the test section is visible and the experimental phenomena could be easily observed and recorded by a digital camera.

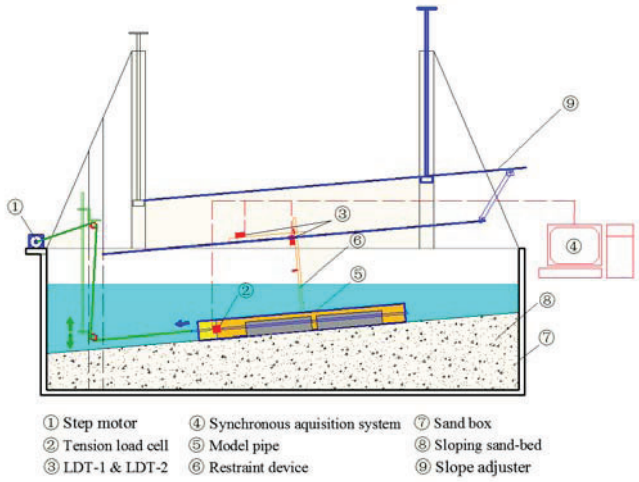

Fig.2 Mechanical-actuator system for modeling axial pipe-soil interaction on a sloping sand-bed.

A displacement-controlled loading system was adopted for the mechanical-actuator experiment. The external axial load was applied on the model pipe by the step motor through a stainless steel cable. In the axial loading tests, the model pipe moved axially with a constant velocity of about 13 mm/s.

The saturated sloping sand bed was made of medium silica sand, of which $d_{50} = 0.38\,\text{mm}$, $d_{10} = 0.30\,\text{mm}$, $C_u = 1.46$, $D_r = 0.32$, $\gamma' = 9.03\,\text{kN/m}^3$, $\phi = 35^\circ$, $C_V = 0.154\,\text{m}^2/\text{s}$. The slope angle α is in the range of $-9^\circ \sim +9^\circ$. The value of α is positive when the model pipe moves upward along the sand bed while negative value for the downward movement.

The model pipe was 0.20 m in diameter, 2.20 m in length. The dimensionless submerged pipe-weight G varied from 0.34 to 0.82 . The relative pipe roughness λ was in the range of 0~0.18 . Axial rotation was restricted by a restraint device installed on the model pipe.

The pipe consisted of the pipe-cap (0.20 m long, connected with the cable, marked with yellow in Fig.2) and the test section (2.00 m long, marked with orange).

The tension load cell, which was used to measure the external axial force, was placed between the pipe-cap and test section. That is, the tension load cell measured only the axial loading on the test section and the effect of end-resistance was therefore eliminated during the test. The external force F_{Du} can be regarded as the anti-slide capacity F_A if the model pipe moves at a constant speed. Two laser displacement transducers (LDTs) were employed for the measurement of pipe displacements parallel and perpendicular to the slope respectively. The LDTs and the tension load cell were triggered by the synchronous acquisition system, by which the loading and displacement could be recorded synchronously.

The testing procedure was as follows: (1) the model pipe was laid along the slope and the initial settlement was measured with the laser displacement transducer; (2) the model pipe was pulled axially with a constant velocity by the step motor, the axial displacement, settlement and the external loading was recorded; (3) the model pipe was lifted to its original position and the step (2) was repeated until no significant change of the measured data was observed. The aforementioned procedure was recorded with a digital camera during the tests.

In this study, the slope angle α , the submerged pipe-weight G and the pipe-roughness λ are chosen as the main experimental variables. The experimental conditions are listed in Table 1.

Table 1. Experimental conditions.

Test no.	W_S (N/m)	G	d_p (μm)	λ	α (°)
W1R0S0	123	0.341	≈0	≈0	0
W2R0S0	144	0.399	≈0	≈0	0
W3R0S0	165	0.457	≈0	≈0	0
W4R0S0	186	0.515	≈0	≈0	0
W5R0S0	208	0.576	≈0	≈0	0
W6R0S0	230	0.637	≈0	≈0	0
W7R0S0	251	0.695	≈0	≈0	0
W8R0S0	272	0.753	≈0	≈0	0
W9R0S0	294	0.814	≈0	≈0	0
W7R0S0	251	0.695	≈0	≈0	0
W7R1S0	251	0.695	10	0.026	0
W7R2S0	251	0.695	18	0.047	0
W7R3S0	251	0.695	69	0.182	0
W7R0S+1	251	0.695	≈0	≈0	3
W7R1S+1	251	0.695	10	0.026	3
W7R3S+1	251	0.695	69	0.182	3
W7R0S+2	251	0.695	≈0	≈0	6
W7R1S+2	251	0.695	10	0.026	6
W7R3S+2	251	0.695	69	0.182	6
W7R0S+3	251	0.695	≈0	≈0	9
W7R1S+3	251	0.695	10	0.026	9
W7R3S+3	251	0.695	69	0.182	9
W7R0S-1	251	0.695	≈0	≈0	-3
W7R3S-1	251	0.695	69	0.182	-3
W7R0S-2	251	0.695	≈0	≈0	-6
W7R3S-2	251	0.695	69	0.182	-6
W7R0S-3	251	0.695	≈0	≈0	-9

EXPERIMENTAL RESULTS AND DISCUSSIONS

Typical Features of the Axial Pipe-soil Interaction

Figs.3a-3e illustrate the loading curves of the smooth pipe on a horizontal sand bed. The pipe was static for $s/D<0$. The moving average of the external load (cyclic) F_D is used for interpreting the axial soil-resistance (F_{Ru}) and the anti-slide capacity (F_A).

For the smooth pipe ($\lambda \approx 0$) , the phenomenon of "pipe-trembling" is observed in most of the tests: the movement of the model pipe contains breaks, which means the model pipe suddenly moves from static status and then back to static status, the model pipe is in continuous "move-pause-move" state. It should be noted that the pause state is quite short. As the "pipe-trembling" occurs, the fluctuation of the external loading at a certain frequency is observed at the same time, which is shown in Fig.3(a-e). Besides, the increase of F_{Am} in Fig.3(a-e) indicates that the phenomenon of "pipe-trembling" is insignificant in the beginning but becomes more significant when the loading times and the accumulative axial displacement $\Sigma(s/D)$ increase, which is also confirmed by experimental observation. In some other tests, the "pipe-trembling" even doesn't occur at the early part of the 1st loading.

It can be observed in a single loading curve (e.g. Fig. 3(a-e)) that firstly the axial soil-resistance reaches its maximum value F_{Br} when the model pipe begins to move, and then gradually decreases with the development of axial displacement (s) . The residual soil-resistance F_{Re} decreases firstly with the increase of the loading times, and then keeps constant when $\Sigma(s/D)>8$.

In the studies of the soil-resistance and anti-slide capacity of a pipeline on a horizontally-flat seabed by Bruton et al. (2008) and Randolph et al. (2012), the decrease of F_A is mainly due to the excess pore pressure generated at the pipe-soil interface, which is caused by the contractive volumetric strain of the neighboring soil. However, in this study, the tests are under drained condition for $VD/C_V \approx 1.69\times10^{-2}$. Therefore, the mechanism of the decrease of F_A would be different, which is to be discussed in the next section.

The experimental results for the rough pipes are different from the smooth pipes (see Fig. 3(f)). The anti-slide capacity F_A for rough pipes is much larger than that for smooth pipes. The value of F_{Re} varies slightly for different loading times. However, unlike the smooth pipe, the variety of F_{Re} for the rough pipe is not monotonic with the increase of loading times.

Two types of loading curves can be obtained for the rough pipe: (1) a peak value of F_A is found when the model pipe begins to move, and F_A quickly decreases to a lower value after the breakout; (2) the peak value doesn't exist. Type (1) is more prone to occur when $\Sigma(s/D)<5$. However, as $\Sigma(s/D)$ increases, the maximum value gradually decreases, and finally type (2) may appear when $\Sigma(s/D)>7$. Compared with the smooth pipe, the loading curves of rough pipes are generally smooth and no "pipe-trembling" was observed in all the tests.

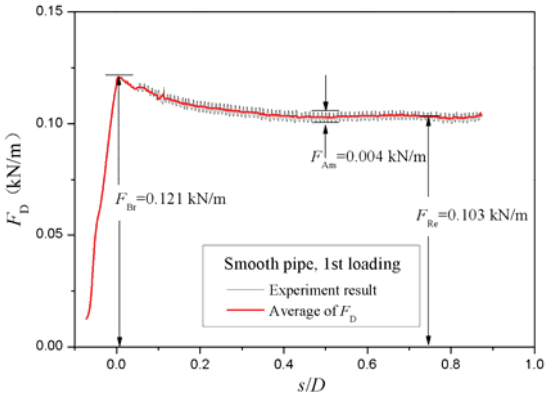

(a)

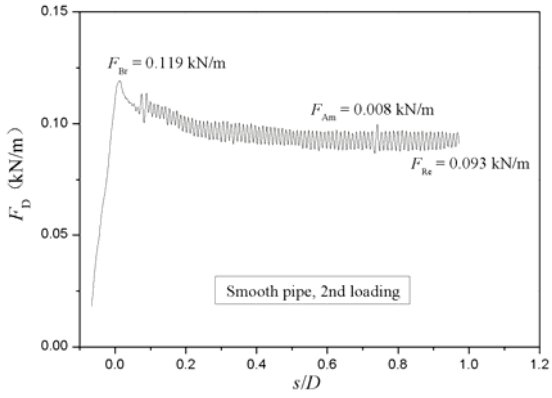

(b)

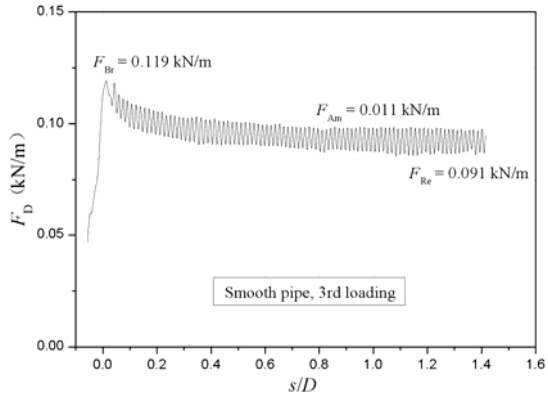

(c)

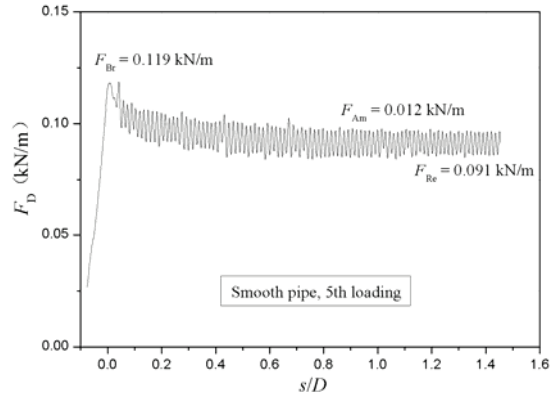

(d)

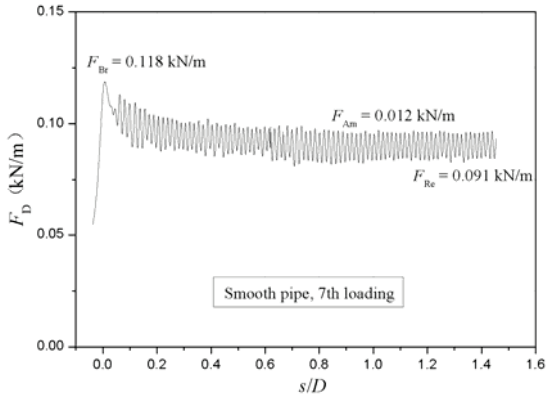

(e)

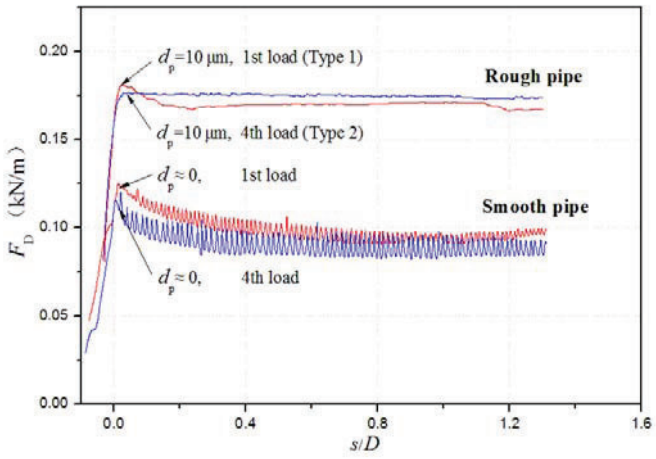

(f)

Fig.3 The loading curves for rough and smooth model pipe:
(a-e): smooth pipe (test no. W7R0S0); (f): rough pipe (test no. W7R1S0).

Effects of Pipe-roughness

The development of pipe settlement with $\Sigma(s/D)$ is illustrated in Fig.4. It can be seen that with the increase of $\Sigma(s/D)$, the final settlement of rough pipes is approximately twice as that of smooth pipes. However, for the rough pipes with different roughness $(0 \le \lambda \le 0.182)$, the settlements are almost the same.

From Fig.3, Fig.4 and Table 2, we know that the differences of the loading curve, pipe settlement and the residual anti-slide capacity are significant between the smooth and rough pipe. However, for the value of d_p in range of 10~69 μm ($0.026 \le \lambda \le 0.182$), the influence of pipe roughness can be ignored, which means that the pipe-soil interaction mode may be changed when d_p ranges from 0 to 10 μm .

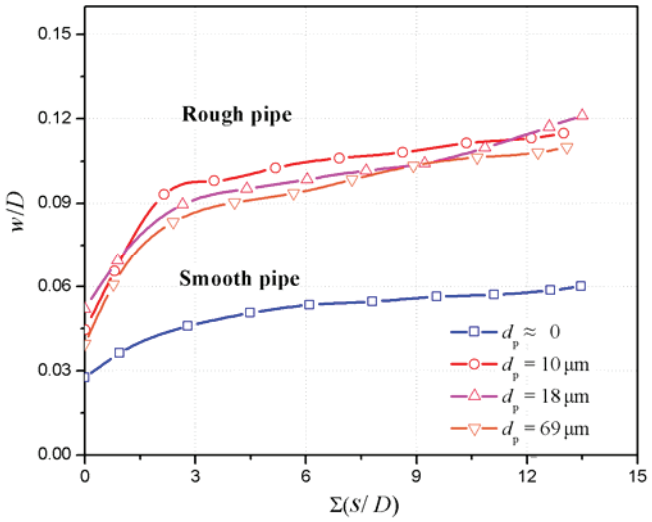

Fig. 4 The pipe settlement vs. accumulative axial displacement on a horizontal sand-bed. (Test no. W7R0S0—W7R3S0)

Table 2. The average value of F_{Re} for different pipe roughness on horizontal sand-bed. (Test no. W7R0S0—W7R3S0)

d_p (μm)	≈ 0	10	18	69
λ	≈ 0	0.026	0.047	0.182
F_{Re} (kN/m)	0.085	0.174	0.173	0.175
ζ	0.339	0.693	0.689	0.697

A planar shearing test was conducted to further investigate the pipe-soil interaction, as shown in Fig.5. The plate on the sand-bed was pulled horizontally at the speed of about 10 mm / s , and the displacement is 70 mm . The normal contact force on the pipe-soil interface is about 1.6 kPa . The medium sands on the interface are partially colored with black to show the movement of the sand grains. The test results are given in Fig.6.

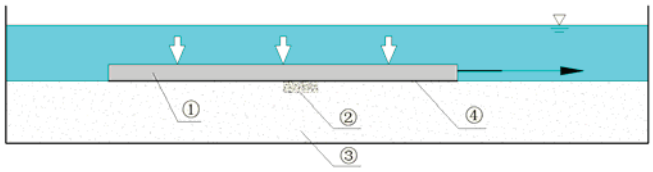

① Plate ② Colored sand ③ Saturated sand ④ Smooth/Rough surface

Fig.5 The planar shearing test for different roughness of interface.

As illustrated in Fig.6 (a), most of the sand grains remained in their initial positions after shearing with the smooth plate surface and little plastic deformation existed in the sand-bed. However, for the rough plate, the displacement of the sand grains is 64 mm (about 91% of the plate's displacement), indicating most of the sand grains on the interface were moving with the plate at almost the same speed. Therefore, the pipe-soil friction mainly exists in the plastic zone of the soil for the rough pipes.

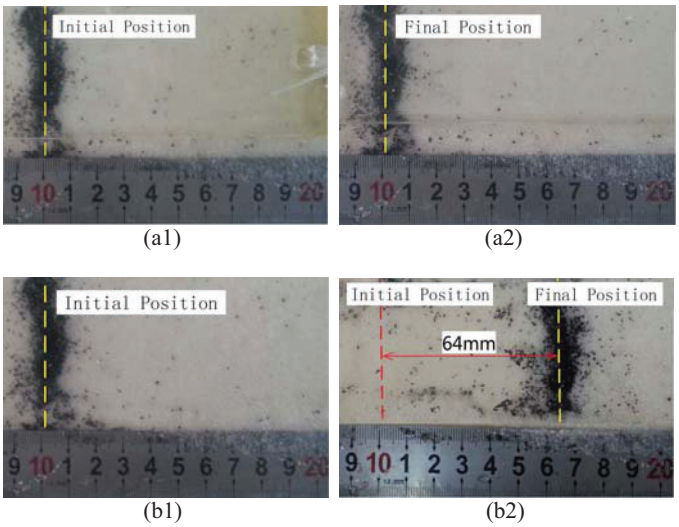

(a1) (a2)

(b1) (b2)

Fig.6 The movement of the sand grains on the interface: (a) smooth surface, $\lambda \approx 0$; (b) rough surface, $\lambda = 0.026$.

Based on the results of planar shearing test, some features of Table 2 and Fig.3 can be explained as follows:

The value of anti-slide capacity ζ

For the pipe with smooth surface, the sand-bed is in static condition and the energy is consumed only on the pipe-soil interface. For the rough pipe, much energy dissipates in the plastic zone of the sand-bed, which makes the soil-resistance of rough pipe much larger than that of smooth pipe. Because the axial friction for the rough pipe mainly exists in the plastic zone of soil rather than the pipe-soil interface, the soil-resistance is mainly determined by ϕ and W_S while the effect of pipe roughness can be ignored.

We suppose that the friction coefficient $\mu = \tan\phi$ for the rough pipe. Referring to White & Randolph (2007) and Eq.(2), the theoretical value of ζ is 0.700 (regardless of the "wedge effect") and 0.753 (considering the "wedge effect") respectively. Compared with Table 2, the theoretical solution for ζ considering the "wedge effect" is about 9% larger than the experimental results. This may because that the newly prepared silica sand on the surface is loose and bears a pressure

of no more than 2kPa during the text, the density of the sand is smaller than the sample of the triaxial tests. Therefore, the actual ϕ of the sand is smaller than 35°.

The mechanism of the "pipe trembling"

For the smooth pipe, when the model pipe is pulled by the external loading, the strain-energy will be firstly accumulated at the contact points between the pipe-surface and the sand grains. After reaching its maximum value, the energy is suddenly released with the pipe's breakout at a high speed. The sudden breakout of pipe loosens the steel cable and the model pipe decelerates due to the soil-resistance. The repeat of breakout-deceleration finally appears as the phenomenon of "pipe trembling". The more sand grains reach the maximum strain-energy at the same time, more significant the "pipe-trembling" phenomenon can be observed.

However, the "pipe-trembling" is impossible for the sand-bed in which the sand grains keep moving and rotating when sheared by a rough surface and are in different energy states respectively. During the first loading of smooth pipe, the newly prepared sand-bed is very loose and is in the process of becoming denser. Similar to the rough pipe, the sand grains are not static. That's why even for the smooth pipe, the "pipe-trembling" phenomenon is not significant during the first loading.

The decrease of anti-slide capacity ζ

When sheared by smooth pipe-surface, the sand grains on pipe-soil interface may be adjusted by slight rotation to make the resistance smaller. For the loose sand-bed, the adjusting time is delayed as the sand-bed becomes denser. As a result, the value of F_{Re} gradually decreases with the increase of loading times.

For the rough pipe, because the mechanism of pipe-soil interaction is totally different, the variety of F_{Re} is no longer monotonic with the loading times.

Effects of Submerged Pipe-weight

The relationship between the dimensionless anti-slide capacity ζ and submerged pipe-weight G is given in Fig. 7. It can be seen that the value of ζ increases slightly with the increase of G.

Assuming that ζ is linearly correlation with G, the anti-slide capacity of smooth pipe can be therefore expressed as:

$$\zeta|_{\alpha=0} \approx a_1 G + a_2 \tag{4}$$

in which a_1 and a_2 are the dimensionless fitting parameters. In this study, $a_1 = 0.084$, $a_2 = 0.260$.

It should be noted that Eq.(4) is only for the case $0.341 < G < 0.814$. When $G \to 0$ or $G \to \infty$, the relationship may no longer be linear.

In the process of the axial pipe-soil interaction, a heavier pipe may lead to a larger value of the pipe settlement. Referring to Eq. (2), the axial anti-slide capacity ζ is in positive correlation with G due to the "wedge effect", which agrees with Fig.7. However, the value of $\zeta_{W9R0S0}/\zeta_{W1R0S0}$ derived by Eq.(4) is 113.8%, which is much larger than the value predicted with Eq.(2) (103.6%), and the fitting line of ζ/κ is not horizontal. It may be because the pipe-weight G influences not only the wedge effect but also the density of the sand and therefore, the friction coefficient μ.

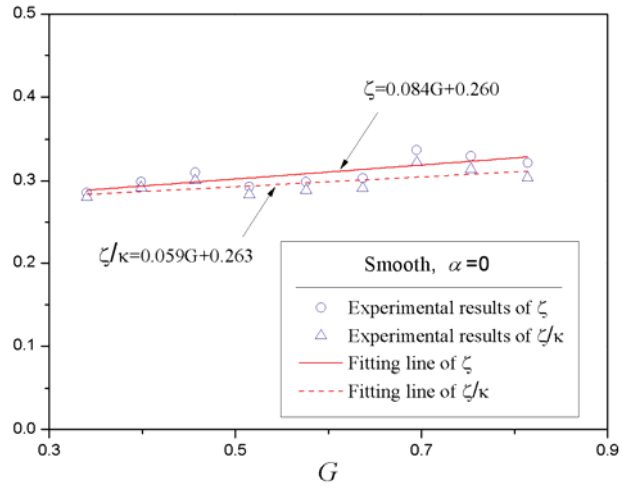

Fig.7 The effect of submerged pipe-weight on the anti-slide capacity. (Test no. W1R0S--W9R0S0)

Effects of Slope Angle

Fig.8 shows that the axial anti-slide capacity factor ζ is greatly affected by the slope angle α for both the rough and smooth model pipe with a certain value of the submerged pipe-weight.

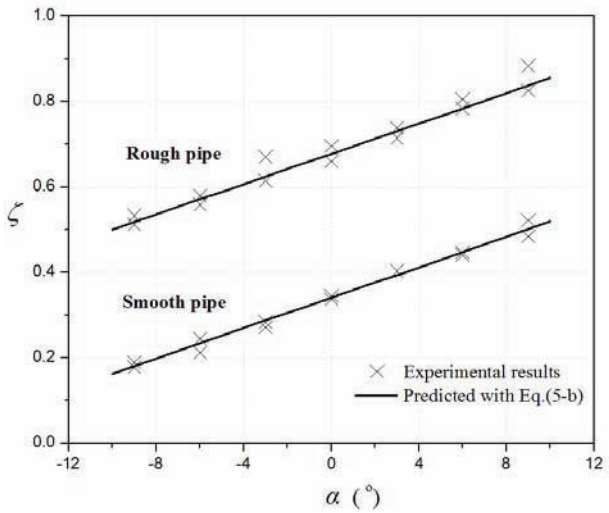

Fig.8 The anti-slide capacity ζ affected by α. (Test nos. W7R0S-3--W7R0S+3, W7R3S-3--W7R3S+3)

In the lateral pipe-soil interaction (Gao et al., 2012), the anti-slide capacity of pipeline was expressed as:

$$F_A = \eta W_S \cos\alpha + W_S \sin\alpha \tag{5a}$$

$$\zeta = \eta + \tan\alpha \tag{5b}$$

in which, $\eta = F_{Ru}/W_S \cos\alpha$ is the coefficient of soil-resistance. For a constant value of η with the slop angle increase from $-9°$ to $+9°$, the

$\zeta - \alpha$ curves predicted with Eq.(5-b) are given in Fig. 8. It's shown that the curves match well with the experimental results, which indicates that the coefficient of soil resistance η can be assumed as constant in the examined range of slope angle ($-9^0 < \alpha < 9^0$) .

However, in Gao et al. (2012), the value of η is greatly influenced by α for the model pipe moving laterally along the sloping sand-bed. Such a difference may be due to the coefficient of lateral soil-resistance being affected by the passive soil-resistance (see Wagner et al. 1989 and Randolph et al. 2011), which is sensitive to the slope angle.

Substituting Eq. (4) into Eq. (5b) to take into account of the effect of λ, the dimensionless axial anti-slide capacity ζ is therefore expressed as follows:

$$\zeta \approx a_1 G + a_2 + \tan\alpha \tag{6}$$

where the dimensionless fitting parameters a_1 and a_2 are functions of λ. That is:

$$a_1 = \begin{cases} f_1(\lambda) & (0 < \lambda < \lambda_s) \\ const1 & (\lambda_s \le \lambda \le \lambda_r) \end{cases} \tag{7a}$$

$$a_2 = \begin{cases} f_2(\lambda) & (0 < \lambda < \lambda_s) \\ const2 & (\lambda_s \le \lambda \le \lambda_r) \end{cases} \tag{7b}$$

in which, $f_1(\lambda)$ and $f_2(\lambda)$ are the increasing functions of λ. λ_s is a threshold value of λ. Referring to the experimental results, $\lambda_s \le 0.026$. This is approximately 25% of the value published by Kishida and Uesugi (1987). When $\lambda_s \le \lambda < \lambda_r$, the friction mainly exists in the plastic zone of the soil and the anti-slide capacity is uncorrelated with λ. λ_r is the upper limit of λ. For $\lambda > \lambda_r$, the geometry of the pipe is affected by λ and the outline of pipe section can be no longer regarded as perfectly circular compared with the size of sand grains.

CONCLUDING REMARKS

A mechanical-actuator system has been specially designed for investigating the pipe-soil interaction on a sloping sandy seabed. The effects of the pipe roughness, submerged pipe-weight and the slope angle on the anti-slide capacity are investigated through the mechanical-actuator loading tests.

The interaction behaviors between the partially-embedded pipeline and its surrounding soil depend on the pipe-soil interface condition and on the development of the plastic zone in the soil. The phenomenon of "pipe-trembling" may occur for smooth pipes rather than the rough pipes. The pipe roughness greatly affects the dimensionless anti-slide capacity factor and the pipe-settlement. For the horizontal sandy seabed, the submerged pipe-weight has slight effect on the axial anti-slide capacity factor and the coefficient of soil resistance. The slope angle affects the anti-slide capacity mainly by the down-slope component of pipe-weight. Unlike the lateral pipe-soil interactions, the slope angle has slight effect on the axial soil resistance to the partially-embedded pipeline in the examined range of slope angle ($-9^o \sim +9^o$).

ACKNOWLEDGEMENTS

This study was financially supported by the National Natural Science Foundation of China (Grant no. 11372319). Technical assistances from Mr. Hai-yang Jiang (master student) and Mr. Fu-lin Zhang in the experimental facility design and tests are greatly appreciated.

REFERENCES

Bruton, DAS, White, DJ, Carr, M and Cheuk, JCY (2008). "Pipe-soil interaction during lateral buckling and pipeline walking–the safebuck JIP," *Offshore Technology Conference*, Houston, OTC-19589.

Chatterjee, S, White, DJ and Randolph, MF (2013). "Coupled consolidation analysis of pipe-soil interactions," *Canadian Geotechnical Journal*, 50, 609-619.

Cheuk, CY, White, DJ and Bolton MD (2007). "Large-scale modeling of soil-pipe interaction during large amplitude cyclic movement of partially embedded pipelines," *Canadian Geotechnical Journal*, 44, 977-996.

Det Norske, Veritas (2007). "On-bottom stability design of submarine pipelines," *Recommended Practice*, DNV-RP-F, 109.

Gao, FP, Han, XT, Cao, J, Sha, Y and Cui, JS (2012), "Submarine pipeline lateral instability on a sloping sandy seabed," *Ocean Engineering*, 50, 44-52.

Hobbs, RE (1984). "In service buckling of heated pipelines," *Journal of Transportation Engineering*, Vol 110, 175-189.

Kishida, H and Uesugi, M (1987). "Tests of the interface between sand and steelin the simple shear apparatus ," *Géotechnique*, 37, pp 45-52.

Nasser, D, Shawn, K, Ryan, P and Radu, P (2011). "Investigating pipeline-soil interaction under axial-lateral relative movements in sand," *Canadian Geotechnical Journal*, 48, 1683-1695.

Quinn, TAC and Brown, MJ (2011). "Effect of strain rate on isotropically consolidated kaolin over a wide range of strain rates in the triaxial apparatus," *International Symposium on Deformation Characteristics of Geomaterials*, Seoul, 607-613.

Randolph, MF, Gaudin, C, Gourvenec, SM, White, DJ, Boylan, N and Cassidy, MJ (2011). "Recent advances in offshore geotechnics for deep water soil and gas developments," *Ocean Engineering*, 38, 818-834.

Randolph, MF, White, DJ and Yan, Y (2012). "Modelling the axial soil resistance on deep-water pipelines," *Géotechnique*, 62, pp 837-846.

Schaminee, PE, Zorn, NF and Schotman, GJM (1990). "Soil response for pipeline upheaval buckling analyses: full scale laboratory tests and modeling," *22nd Annual Offshore Technology Conference*, Houston, OTC, 563-572.

Wagner, DA, Murff, JD, Brennodden, H and Sveggen, O (1989). "Pipe-soil interaction model," *Journal of Waterway, Port, Coastal and Ocean Engineering*, 115(2), 205-220.

White, DJ and Randolph, MF (2007). "Seabed sharacterisation and models for pipeline-soil interation," *Proceedings of the Seventeenth International Offshore and Polar Engineering Conference*, Lisbon, ISOPE, 2, 758-769.